ACS APPLIED MATERIALS & INTERFACES

Research Article

www.acsami.org

Fe_3O_4/Fe/Carbon Composite and Its Application as Anode Material for Lithium-Ion Batteries

Xiuyun Zhao,[†] Dingguo Xia,*[,‡] and Kun Zheng[§]

[†]College of Environmental and Energy Engineering and [§]Institute of Microstructure and Properties of Advanced Materials, Beijing University of Technology, Beijing 100124, China

[‡]College of Engineering, Peking University, Beijing 100871, China

ABSTRACT: A plum pudding-like Fe_3O_4/Fe/carbon composite was synthesized by a sol−gel polymerization followed by a heat-treatment process and characterized by X-ray diffraction, Raman spectroscopic analysis, thermogravimetric analysis, scanning electron microscopy with energy-dispersive spectroscopy, transmission electron microscopy, and electrochemical test. In this composite, uniform spherical Fe_3O_4/Fe nanoparticles of about 100 nm were embedded into carbon matrix with high monodispersion. As-prepared Fe_3O_4/Fe/carbon composite electrode exhibits a stable and reversible capacity of over 600 mA h g^{-1} at a current of 50 mA g^{-1} between 0.002 V and 3.0 V, as well as excellent rate capability. The plum pudding-like structure, in which trace Fe promotes conductivity and carbon matrix mediates the volume change, can enhance the cycling performance and rate capability of Fe_3O_4 electrode. This unique structure is valuable for the preparation of other electrode materials.

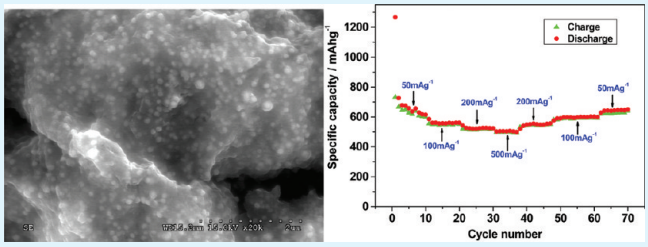

KEYWORDS: *Fe_3O_4/Fe/carbon composite, plum pudding-like structure, anode material, lithium ion battery*

1. INTRODUCTION

Since the first commercialization by Sony Corporation in the early 1990s, lithium-ion batteries have conquered portable electronic market for their high energy density per unit volume or per unit mass and output voltage. As a prime candidate to power the next generation of electric vehicles (EVs) and plug-in hybrid electric vehicles (PHEVs), lithium ion batteries are widely investigated to meet the increasing requirements. In the quest for better batteries, various novel negative materials have been developed since commercial graphite has already approached its theoretical limit of C_6Li (372 mA h g^{-1}). Among these alternatives, nanosized transition-metal oxides (MO, M = Co, Ni, Cu, Fe, or Mn) have intrigued many researchers due to their high electrochemical capacities from the conversion mechanism ($MxOy \leftrightarrow M + Li_2O$) instead of the intercalation reaction.[1] For example, Fe_3O_4 anodes are attracting growing attention for its high theoretical specific capacity (926 mA h g^{-1}, $Fe_3O_4 + 8Li^+ \leftrightarrow 4Li_2O + 3Fe$), safety (a slightly higher voltage plateau), high electronic conductivity, nature abundance (low cost), and environmental benignity.[2−4] However, a large specific volume change commonly occurs in the host matrices of these metal oxides during the cycling process, thus leading to pulverization of electrodes and rapid capacity decay. In previous research, two main kinds of strategies have often been considered: (1) The design of nanostructured materials (rods,[2,5−8] fiber,[9] wires,[3] spheres,[10,11] film,[12] and so on) is an effective path to reduce the absolute volume change and offer a shorter diffusion length for lithium ion leading to enhanced discharge/charge rates. (2) The other strategy is to use a "buffer" matrix to accommodate large volume changes and prevent active nanoparticles from aggregating. Carbon is a commonly used matrix, because of its good ionic conductivity, low volume expansion, and tolerance to mechanical stress. To achieve these strategies, researchers have previously tried many methods to create composites of active materials embedded in carbon matrices, including hydrothermal/solvothermal reaction,[2,3,6,10,13−22] electrospinning,[9] chemical deposition,[23−28] impregnation,[29,30] etc. Despite the above successful demonstrations, the preparation of a new type transition-metal oxide/matrix composite with a well-defined shape is still highly desirable and technologically important.

Herein, we successfully synthesized an Fe_3O_4/Fe/carbon composite with a unique structure of Plum Pudding by a sol−gel polymerization followed by a heat-treatment process. The synthetic procedure is applicable for large-scale production of metal oxide/carbon composites. In the resulting composite, uniform spherical Fe_3O_4/Fe nanoparticles of about 100 nm were embedded into carbon matrix with highly monodispersion. The content of Fe_3O_4/Fe is about 54% by weight, so carbon matrix can efficiently accommodate the volume change of the conversion reaction and provide continuous conductive networks, protecting electrode from pulverization. When used as anode materials in lithium ion batteries, as-prepared Fe_3O_4/Fe/carbon composite shows excellent electrochemical proper-

Received: November 18, 2011
Accepted: February 2, 2012
Published: February 2, 2012

ties in terms of high-rate charge/discharge performance and cyclability.

2. EXPERIMENTAL SECTION

Materials Synthesis. The Fe_3O_4/Fe/carbon Composite was prepared using a simple sol−gel method followed by a heat-treatment process. In a typical synthesis, 0.09 g of cetyltrimethylammonium bromide (CTAB) was dispersed in 100 mL of deionized water with the help of ultrasonication. Then, the mixture of resorcinol (R, 0.11 g), a 37−40 wt % solution of formaldehyde in water (F, 75 g), and sodium carbonate (0.002 g as a catalyst for RF sol−gel polymerization) was added to obtain RF sols. Next, 0.706 g of $Fe(acac)_3$ was added to the above colloids. This sol was then polymerized at 85 °C for 3 days to obtain the $Fe(acac)_3$/RF polymer. After drying in an oven at 85 °C, the product was heat-treated at 600 °C for 1 h under nitrogen atmosphere to carbonize the RF polymer and to get Fe_3O_4/Fe/carbon composite. For comparison, pure carbon was prepared in a similar manner except $Fe(acac)_3$ was absent, and Fe_3O_4/carbon composite not containing Fe was also prepared at 500 °C.

Materials Characterization. X-ray diffraction (XRD) patterns were recorded with a German Bruker D8 advance diffractometer equipped with a Cu anticathode (Cu Kα radiation λ =1.54056 Å) at room temperature. Transmission electron microscopy (TEM) and scanning electron microscopy (SEM) analysis were carried out, respectively, with a JEOL JEM-2010F TEM and a Hitachi S-4300 SEM with an EDAX GENESIS XM2 60S energy-dispersive spectroscopy analyzer. Raman spectroscopic analysis was performed with a Renishaw In-Via System utilizing a 514.5 nm incident radiation and a 50× aperture (N.A = 0.75), resulting in an ~2 μm diameter sampling cross-section. X-ray photoelectron spectroscopy (XPS) spectra were obtained using a Kratos Axis Ultra System with monochromatic Al Kα X-rays (1486.6 eV) at 15 kV and 15 mA (emission current) in a chamber with a base pressure of approximately 1 × 10^{-8} Pa. Thermogravimetric analysis (TGA) was carried out on a TG/DTA6300 thermal analyzer with a heating rate of 5 °Cmin^{-1} in flowing N_2 or air atmosphere.

Electrochemical Characterization. Electrochemical performances were evaluated with CR2032 coin cells with a Neware System. The test electrodes were prepared by mixing 80 wt % composite material with 10 wt % acetylene black as a conductive agent and 10 wt % polymer binder (polyvinylidene fluoride, PVDF) as a binder to form slurry, which was then coated onto a stainless steel foil and pressed and dried under vacuum at 80 °C for 12 h. The coin cells were finally assembled in an argon filled glovebox with the Fe_3O_4/Fe/carbon (or pure carbon) test electrode, metallic lithium as the counter and reference electrode, 1 M $LiPF_6$ in 1:1 diethyl carbonate/ethylene carbonate electrolyte, and Whatman GF/D borosilicate glass-fiber sheets as separators. Discharge−charge measurements were carried out galvanostatically at various rates over a voltage range of 0.002 to 3.0 V (vs Li/Li^+). Electrochemical impedance spectra (EIS) were recorded between 200 kHz and 5 mHz with an amplitude of 5 mV on a VMP3 (Princeton Applied Research). Cyclic voltammetry (CV) measurement was conducted at 0.05 mV s^{-1} between 3.0 V and 0.0 V on the same VMP3.

3. RESULTS AND DISCUSSION

The crystal structure of the final products was characterized by XRD and the results are presented in Figure 1a, which match well with those of face-centered Fe_3O_4 (JCPDS no. 65−3107) in addition to the weak peak at about 44° marked with an asterisk correspond to Fe. The broad signal in the range of 20−30° may be due to the presence of amorphous carbon in the composite. It is further confirmed by the Raman spectroscopic analysis in Figure 1b, which indicates a D-band at 1341 cm^{-1} and a G-band at 1595 cm^{-1} for carbon. Take into consideration the similarity of XRD patterns between Fe_3O_4 and Fe_2O_3, XPS measurement was used to assign the crystal phase of as-

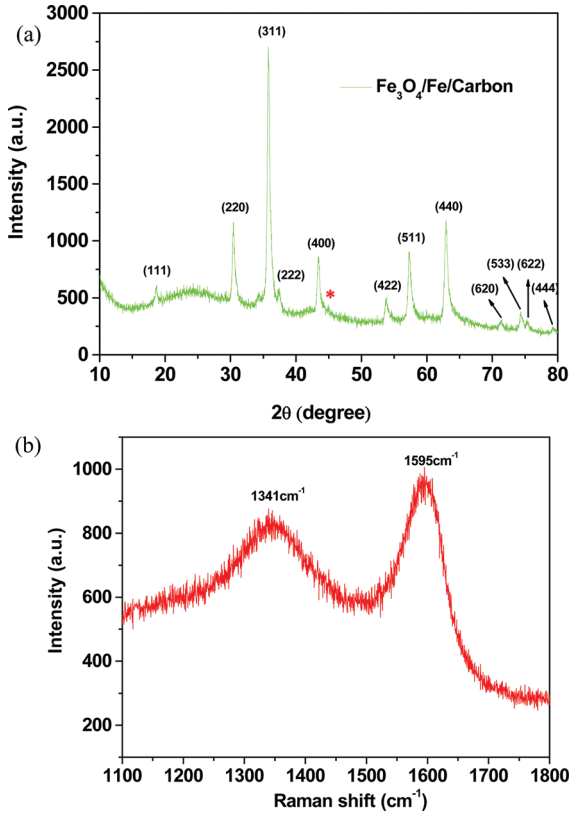

Figure 1. (a) XRD and (b) Raman spectra of Fe_3O_4/Fe/carbon composite.

prepared composite. Figure 2 shows the Fe 2p high-resolution XPS spectrum, in which only two broad peaks (724.8 and 711.3

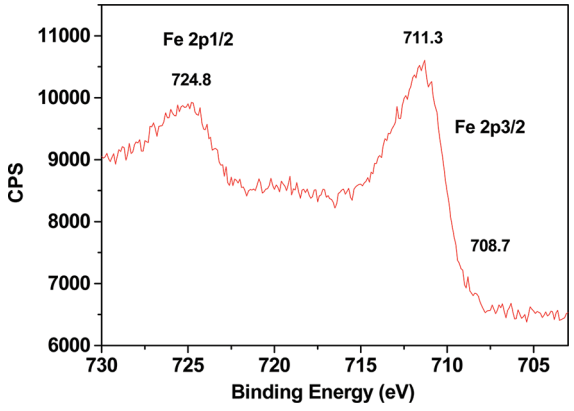

Figure 2. XPS from Fe_3O_4/Fe/carbon composite.

eV) can be observed corresponding to Fe 2p1/2 and Fe 2p3/2 for Fe_3O_4. There is no satellite peak at about 719 eV, which is characteristic for Fe_2O_3, further confirming the Fe_3O_4 phase.[18] Moreover, the weak Fe 2p3/2 peak at around 708.7ev refers to trace Fe of composite.[31] It can be concluded that $Fe(acac)_3$ in the Resorcinol Formaldehyde (RF) sol−gel was converted to Fe_3O_4 and trace amounts Fe when heat-treated at 600 °C under nitrogen atmosphere with the presence of carbon precursor.

The microstructure of the sample is revealed by SEM and TEM analysis shown in Figures 3 and 4. Figure 3b shows the energy-dispersive X-ray spectroscopy (EDX) spectrum of the Fe_3O_4/Fe/carbon composite corresponding to the SEM in

dx.doi.org/10.1021/am201617j | ACS Appl. Mater. Interfaces 2012, 4, 1350−1356

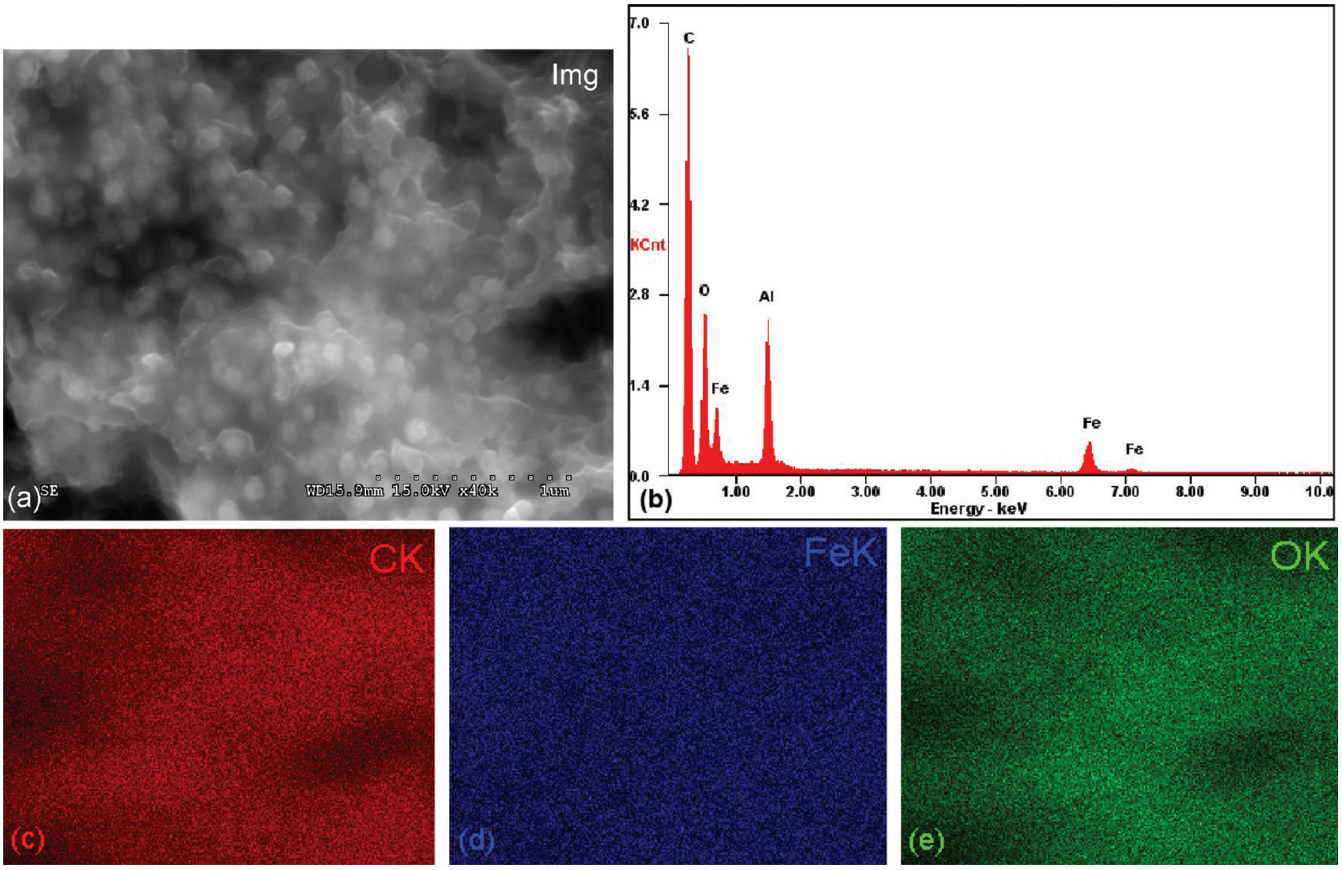

Figure 3. (a) SEM image; (b) EDX spectrum; (c–e) Elemental maps of C, Fe, and O in Fe_3O_4/Fe/carbon composite.

Figure 3a. The peaks corresponding to C, O, Al, and Fe are clearly identified. The peak for Al, comes from the Al-based conductive adhesive supporting the sample. EDX and elemental mapping confirm that the Fe_3O_4 nanoparticless are dispersed uniformly in the carbon matrix. TEM images b and c in Figure 4 clearly show the size of the Fe_3O_4 nanoparticles is about 100 nm, and these roughly spherical nanoparticles are suspended in carbon matrix just like plums in pudding. Figure 4d is a high-resolution TEM (HRTEM) image taken from two contiguous nanoparticles' fringes which reveal a heterogeneous core–shell structure clearly. The *d* spacing of the lattice fringes in the core region is 0.252 nm corresponding to the (311) plane of Fe_3O_4. And a shell about 3 nm in thickness is uniformly coated onto the surface of Fe_3O_4 core. The shell region is indexed to be Fe, based on the interplanar crystal spacing of 0.202 nm along to (110) and the result of XRD index. It indicates the Fe_3O_4 adjacent carbon is partially reduced by the carbon. Because of the low conductivity of carbon from pyrolysis of organic compounds,[32] the presence of trace of Fe on the surface of Fe_3O_4 is helpful for improving the conductivity. We have also taken note that the core–shell nanoparticles with high monodispersion are wrapped by amorphous carbon layer. This unique embedded structure is expected to ensure a good mechanical integrity to Fe_3O_4 material when used as an electrode in lithium ion battery.

Thermogravimetrics (TG) analyses were adopted to disclose the formation process and the carbon content of Fe_3O_4/Fe/carbon composite with plum pudding-like structure. Figure 5a shows the TG and DTG results of the precursor ($Fe(acac)_3$-embedded into RF polymer) heat-treated under N_2 atmosphere. Four obvious valleys can be observed in DTG curve. The first one below 200 °C is ascribed to the loss of water, and the other three are from the chemical reaction. XRD results (not shown here) indicate that Fe_2O_3 starts to generate at 200 °C, and then it is entirely converted into Fe_3O_4 at 500 °C. When the temperature is rased to 600 °C, trace Fe forms with the presence of carbon. The carbon precursor is deduced to start being carbonized at about 270 °C. On the other hand, thermal stability of Fe_3O_4/Fe/carbon composite under air atmosphere is also detected by TG, shown in Figure 5b. The mass of composite keeps almost unchanged below 300 °C, which indicates the composite is stable under atmosphere. With the temperature increase, an obvious weigh loss occurs near 300 °C extending to 420 °C, indicating an oxidation of carbon in the sample. In this process, Fe_3O_4 and trace Fe are transformed into Fe_2O_3, which can bring a small mass increase. It is estimated that the carbon content of Fe_3O_4/Fe/carbon composite is about 46 wt %.

Figure 6a shows the results of discharge–charge galvanostatic cycles of the Fe_3O_4/Fe/carbon composite electrode in the voltage of 0.002 to 3.0 V (vs Li/Li^+). As a comparison, pure carbon electrode prepared by the same procedure was also investigated under the same electrochemical conditions. The theoretical specific capacity of Fe_3O_4 and carbon is 926 and 372 mA h g^{-1}, respectively, so the Fe_3O_4/Fe/carbon composite electrode here has a theoretically calculated specific capacity of 671 mA h g^{-1}. This calculation method of capacity is available in other works in terms of carbon composite electrode.[33−35] Herein, the results indicate that the discharge capacity of the Fe_3O_4/Fe/carbon electrode in the first cycle is as high as 1192 mA h g^{-1} and the corresponding charge capacity is 685 mA h g^{-1} at a 50 mA g^{-1} rate, which exceed the theoretical capacity.

dx.doi.org/10.1021/am201617j | ACS Appl. Mater. Interfaces 2012, 4, 1350−1356

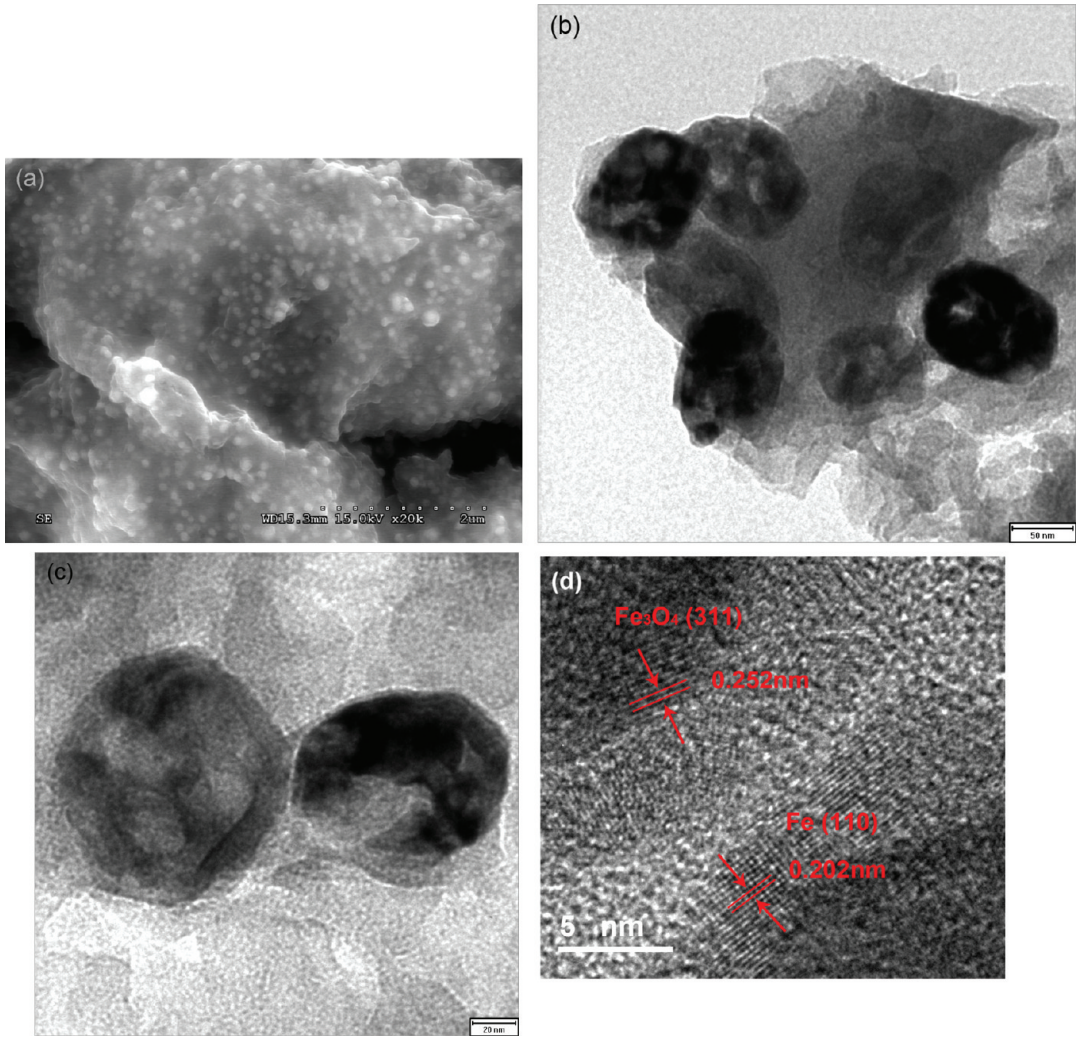

Figure 4. (a) SEM image and (b−-d) TEM images of Fe_3O_4/Fe/carbon composite.

This phenomenon has also been reported for other metal oxides electrode somewhere else,[36−38] which might be attributed to electrolyte decomposition, lithium storage on surface of polymeric layer or interfacial storage.[1] The columbic efficiency is 57% in the initial cycle, after that keeps above 98% in the following discharge−charge cycles. The electrode delivers a very stable specific capacity of above 600 $mAhg^{-1}$ through the subsequent 40 cycles without any decay. The irreversible capacity in the first cycle is usually ascribed to three aspects: First, the formation of solid electrolyte interphase (SEI) films on the electrode surface; Second, lots of oxygen and hydrogen atoms presented in the Fe_3O_4/Fe/carbon composite contribute to the irreversible capacity since this composite was prepared by carbonization of RF polymer at a low temperature of 600 °C.[39,40] Last, the incomplete decomposition of Li_2O from the reaction of Li and Fe_3O_4 is due to the presence of inactive or electrically disconnected Li_2O/Fe regions.[1] These processes consume much Li from the counter electrode. In the first process, the lithium loss is impossible to avoid since SEI films form in the discharge process inevitably. Therefore, increasing reversible formation and decomposition of Li_2O should be taken into consideration to reduce this lithium loss. Kang et al. reported that Ni had the catalytic activity to facilitate Li_2O decomposition in Ni−Co_3O_4 composite electrode.[41−43] Hu et al. have synthesized $Au_{core}Co_3O_{4shell}$ nanocubes anode in which Au as a catalyst decreasing the binding energy of Li_2O.[44] Our group has also used Au to enhance the electronic conductivity of SnO_2 anode.[45] In addition, metallic iron in nanoscale was considered to provide an electronically conductive network and improve the cyclbility of electrode.[46,47] As a comparison, we prepared Fe_3O_4/carbon composite not containing Fe. XRD patterns and cycling performance of Fe_3O_4/carbon composite are shown in panels a and b in Figure 7, respectively. It is found that this composite electrode can only delivers a specific capacity of less than 400 mA h g^{-1} and an initial columbic efficiency of 50% at 50 mA g^{-1}, which are much lower than that of Fe_3O_4/Fe/carbon composite electrode. To find out whether the electrical conduction can be improved by trace Fe in the composite, we conducted an impedance test on two half cells with the Fe_3O_4/Fe/carbon composite and Fe_3O_4/carbon composite as the working electrodes. As shown in Figure 7c, the Fe_3O_4/Fe/carbon composite electrode has much smaller charge-transfer impedance than that of Fe_3O_4/carbon composite electrode. Considering similar electrical conductivity for carbon materials from pyrolysis of organic compounds at 500 and 600 °C,[32] it is deduced that trace Fe of the Fe_3O_4/Fe/carbon composite may improve the electrochemical performance of the electrode.

Figure 6b presents the representative discharge−charge curves of the Fe_3O_4/Fe/carbon composite electrode for the

dx.doi.org/10.1021/am201617j | ACS Appl. Mater. Interfaces 2012, 4, 1350−1356

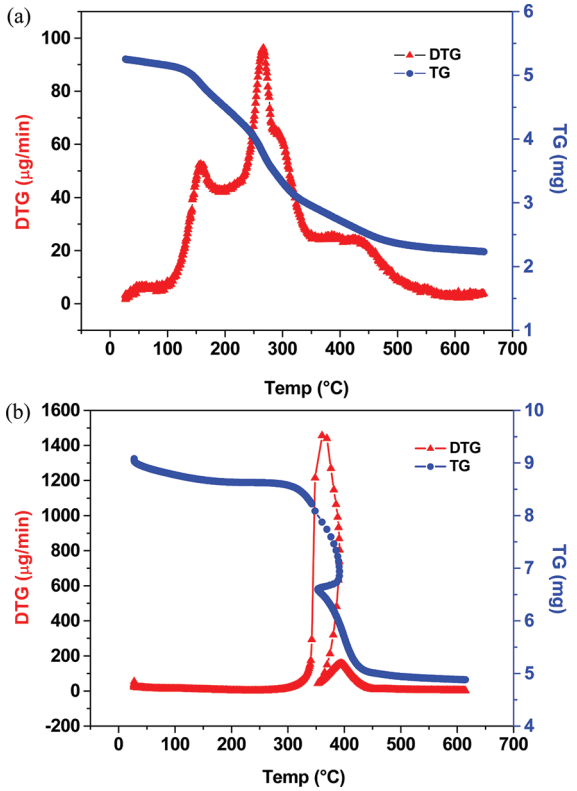

Figure 5. TG results of (a) the precursor under N_2 atmosphere and (b) as-prepared Fe_3O_4/Fe/carbon composite under air atmosphere.

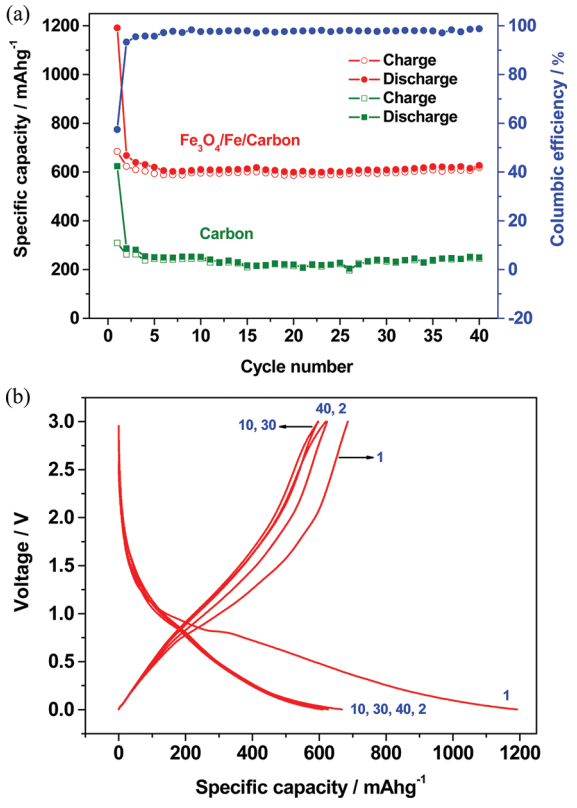

Figure 6. (a) Cycling stability and (b) discharge−charge profiles of Fe_3O_4/Fe/carbon composite electrode.

first, second, 10th, 30th, and 40th cycle at a rate of 50 mA g^{-1}. The discharge voltage first reaches a plateau at about 1.0 V in

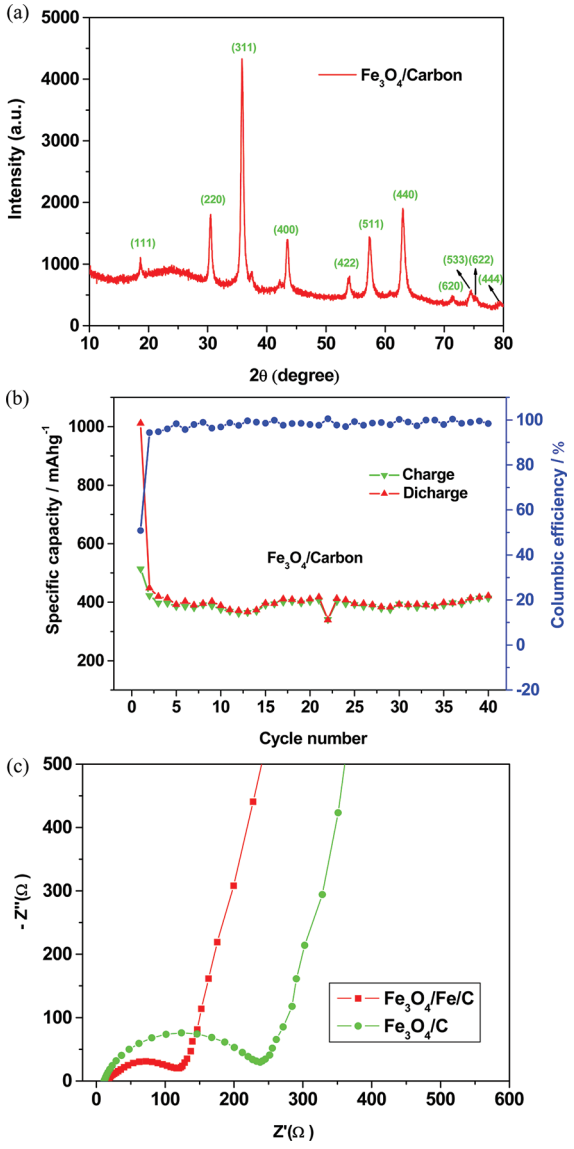

Figure 7. (a) XRD pattern Fe_3O_4/carbon composite, (b) cycling stability of Fe_3O_4/carbon composite electrode at a current of 50 mA g^{-1}, and (c) impedance spectra of Fe_3O_4/Fe/carbon electrode, and Fe_3O_4/carbon electrode.

the first cycle, and then a 0.75 V plateau followed by a long slope, which are ascribed to the formation of SEI on the surface of electrode and the insertion of lithium ions into Fe_3O_4/Fe/carbon composite electrode. During the following discharge process, the average voltage plateau stays at 0.75 V. Besides, the charge curves overlap after the second cycle. As we know, commercial graphite will make a risk of high-surface-area Li plating at the end of recharge, which is associated with safety problems.[48] Herein, the Fe_3O_4/Fe/carbon composite electrode reduces the risk because of its slightly higher voltage plateau.

In addition to the excellent cycling performance, the Fe_3O_4/Fe/carbon composite electrode also shows high rate performance. Figure 8 illustrates the result of cycling at continuously various rates for the same battery. Clearly, the electrode delivers a reversible specific capacity of over 500 mA h g^{-1} at a high rate of 500 mA g^{-1}. When returning to the initial 50 mA g^{-1}, the composite electrode reassumes the original capacity of more than 600A h g^{-1}. These confirm that this electrode can keep its

dx.doi.org/10.1021/am201617j | ACS Appl. Mater. Interfaces 2012, 4, 1350−1356

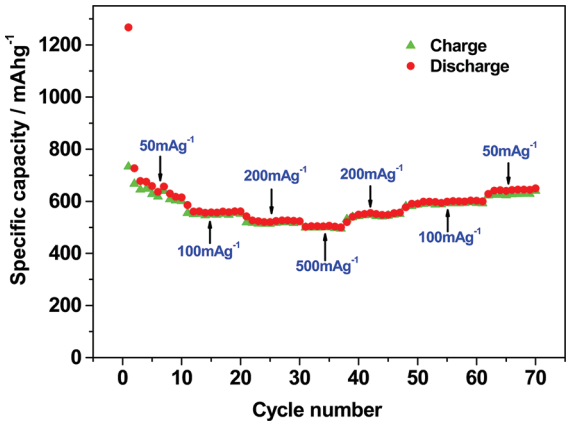

Figure 8. Cycling performance of the same cell at various rates for Fe_3O_4/Fe/carbon composite electrode.

integrity during discharge−charge cycles, which show the good dynamic performance.

Combining the high reversible capacity, excellent cyclic performance, and good rate capability, we believe that this Fe_3O_4/Fe/carbon composite is a potential good candidate as anode material of high-performance lithium-ion batteries. The excellent electrochemical performance of the Fe_3O_4/Fe/carbon composite electrode can be explained as follows: First, Fe_3O_4/Fe nanoparticles with a diameter of about 100 nm have a high active reactivity with lithium and at the same time alleviate the absolute volume changes. Second, the embedded structure of Plum Pudding-like provides large contact surface and good adherence between Fe_3O_4/Fe nanoparticles and carbon matrix, which reduces the diffusion distance of lithium ions and is very helpful for electron and lithium ion conduction. Furthermore, nanosized Fe_3O_4/Fe particles are isolated by the carbon matrix which acts as a barrier to prevent the aggregation of Fe_3O_4/Fe nanoparticles. Both of the two factors are the keys to the excellent performance because they can restrain "pulverization" of electrode. Last, as mentioned earlier, trace Fe of the Fe_3O_4/Fe/carbon composite may catalyze the reversible transfer of Li_2O and enhance the electron conduction networks, thus improving electrochemical performance of electrode.

To further understand the electrochemical process, the cyclic voltammetry (CV) curves of this Fe_3O_4/Fe/carbon composite was recorded for the first four cycles in the voltage range between 3.0 V and 0.0 V at a scan rate of 0.05 mV s^{-1} in Figure 9. In the first cycle, there is a broad peak appears at about 0.50 V in the cathodic process, which can be ascribed to the formation of SEI and the reduction of Fe^{3+} and Fe^{2+} to Fe^0 [29]

$$Fe_3O_4 + Li \rightarrow Fe^0 + Li_2O \quad (1)$$

Two anodic peaks are present at 1.0 V and 1.6 V, corresponding to the oxidation of Fe^0 to Fe^{3+}

$$Fe^0 + Li_2O \rightarrow Fe_3O_4 + xLi \quad (2)$$

In the anodic process, both the peak current and the integrated area of the anodic peak are decreased, indicating capacity loss during the charging process. It is consistent with the results of discharge/charge test. During the subsequent cycles, the cathodic peak potential shifts to about 0.77 V positively with the appearing of a tiny peak at 1.3 V comparing to the first cycle. The anodic peaks shift very slightly. As can be seen, CV

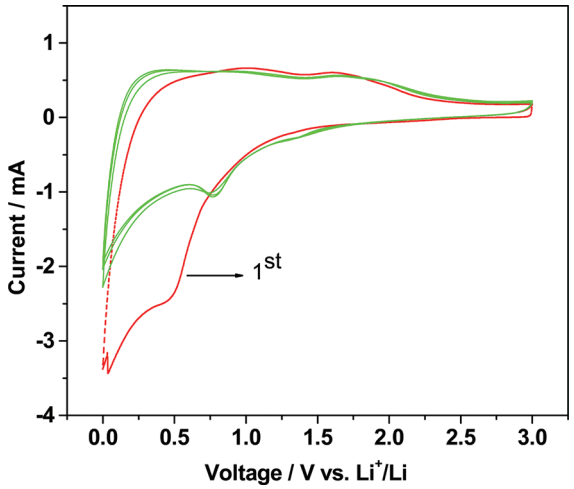

Figure 9. CV of Fe_3O_4/Fe/carbon composite electrode showing the first four cycles between 3.0 V and 0.0 V at a scan rate of 0.05 mV s^{-1}.

curves of the Fe_3O_4/Fe/carbon composite electrode are very stable from the second cycle onward.

4. CONCLUSIONS

In summary, we have successfully synthesized an Fe_3O_4/Fe/carbon composite with a unique structure of Plum Pudding by a sol−gel polymerization followed by a heat-treatment process. In this embedded structure nanosized Fe_3O_4/Fe particles are dispersed uniformly into carbon matrix, which can accommodate volume expansion/contraction of Fe_3O_4 during discharge−charge processes and keep the integrity of electrode. The presence of trace Fe on the surface of Fe_3O_4 particles can further enhance the electron transfer and reduce the resistance within the active nanoparticles. The Fe_3O_4/Fe/carbon composite electrode shows a high reversible capacity (over 600 mA h g^{-1} at a current of 50 mA g^{-1}), excellent cyclic performance and good rate capability, indicting its promising potential as anode material for Li-ion batteries. As a result, this plum pudding-like structure may be extended to other electrode materials including transition-metal oxides, nitrides, sulphides, fluorides, and phosphides in which conversion reactions are common.

AUTHOR INFORMATION

Corresponding Author

*E-mail: dgxia@pku.edu.cn. Tel: +86 10 82529046. Fax: +86 10 67396158.

Notes

The authors declare no competing financial interest.

ACKNOWLEDGMENTS

We gratefully acknowledge financial supports from the major program of Beijing Municipal Natural Science Foundation (20110001) and National Natural Science Foundation of China (11179001).

REFERENCES

(1) Palacin, M. R.; Cabana, J.; Monconduit, L.; Larcher, D. *Adv. Mater.* **2010**, *22*, E170−E192.

(2) Liu, H.; Wang, G. X.; Wang, J. Z.; Wexler, D. *Electrochem. Commun.* **2008**, *10*, 1879−1882.

(3) Muraliganth, T.; Murugan, A. V.; Manthiram, A. *Chem. Commun.* **2009**, 7360−7362.

(4) Taberna, L.; Mitra, S.; Poizot, P.; Simon, P.; Tarascon, J. M. *Nat. Mater.* **2006**, *5*, 567−573.
(5) Ban, C. M.; Wu, Z. C.; Gillaspie, D. T.; Chen, L.; Yan, Y. F.; Blackburn, J. L.; Dillon, A. C. *Adv. Mater.* **2010**, *22*, E145−E149.
(6) Zhu, T.; Chen, J. S.; Lou, X. W. *J. Phys. Chem. C* **2011**, *115*, 9814−9820.
(7) Duan, H. N.; Gnanaraj, J.; Chen, X. P.; Li, B. Q.; Liang, J. Y. *J. Power Sources* **2008**, *185*, 512−518.
(8) Duan, H.; Gnanaraj, J.; Liang, J. Y. *J. Power Sources* **2011**, *196*, 4779−4784.
(9) Wang, L.; Yu, Y.; Chen, P. C.; Zhang, D. W.; Chen, C. H. *J. Power Sources* **2008**, *183*, 717−723.
(10) Wang, S. Q.; Zhang, J. Y.; Chen, C. H. *J. Power Sources* **2010**, *195*, 5379−5381.
(11) Yang, Z. C.; Shen, J. G.; Archer, L. A. *J. Mater. Chem.* **2011**, *21*, 11092−11097.
(12) Mitra, S.; Poizot, P.; Finke, A.; Tarascon, J. M. *Adv. Funct. Mater.* **2006**, *16*, 2281−2287.
(13) Cui, Z. M.; Hang, L. Y.; Song, W. G.; Guo, Y. G. *Chem. Mater.* **2009**, *21*, 1162−1166.
(14) Zhang, W. M.; Wu, X. L.; Hu, J. S.; Guo, Y. G.; Wan, L. J. *Adv. Funct. Mater.* **2008**, *18*, 3941−3946.
(15) Jin, S. L.; Deng, H. G.; Long, D. H.; Liu, X. J.; Zhan, L. A.; Liang, X. Y.; Qiao, W. M.; Ling, L. C. *J. Power Sources* **2011**, *196*, 3887−3893.
(16) Wang, J. Z.; Zhong, C.; Wexler, D.; Idris, N. H.; Wang, Z. X.; Chen, L. Q.; Liu, H. K. *Chem.—Eur. J.* **2011**, *17*, 661−667.
(17) Lian, P. C.; Zhu, X. F.; Xiang, H. F.; Li, Z.; Yang, W. S.; Wang, H. H. *Electrochim. Acta* **2010**, *56*, 834−840.
(18) Wu, P.; Du, N.; Zhang, H.; Yu, J. X.; Yang, D. R. *J. Phys. Chem. C* **2011**, *115*, 3612−3620.
(19) Su, J.; Cao, M. H.; Ren, L.; Hu, C. W. *J. Phys. Chem. C* **2011**, *115*, 14469−14477.
(20) Yuan, S. M.; Zhou, Z.; Li, G. *CrystEngComm* **2011**, *13*, 4709−4713.
(21) Yuan, S. M.; Li, J. X.; Yang, L. T.; Su, L. W.; Liu, L.; Zhou, Z. *ACS Appl. Mater. Interfaces* **2011**, *3*, 705−709.
(22) Chen, J. S.; Zhang, Y. M.; Lou, X. W. *ACS Appl. Mater. Interfaces* **2011**, *3*, 3276−3279.
(23) Zhang, M.; Lei, D. N.; Yin, X. M.; Chen, L. B.; Li, Q. H.; Wang, Y. G.; Wang, T. H. *J. Mater. Chem.* **2010**, *20*, 5538−5543.
(24) He, Y.; Huang, L.; Cai, J. S.; Zheng, X. M.; Sun, S. G. *Electrochim. Acta* **2010**, *55*, 1140−1144.
(25) Zhou, G. M.; Wang, D. W.; Li, F.; Zhang, L. L.; Li, N.; Wu, Z. S.; Wen, L.; Lu, G. Q.; Cheng, H. M. *Chem. Mater.* **2010**, *22*, 5306−5313.
(26) Li, B. J.; Cao, H. Q.; Shao, J.; Qu, M. Z.; Warner, J. H. *J. Mater. Chem.* **2011**, *21*, 5069−5075.
(27) Ji, L. W.; Tan, Z. K.; Kuykendall, T. R.; Aloni, S.; Xun, S. D.; Lin, E.; Battaglia, V.; Zhang, Y. G. *Phys. Chem. Chem. Phys.* **2011**, *13*, 7170−7177.
(28) Chen, D. Y.; Ji, G.; Ma, Y.; Lee, J. Y.; Lu, J. M. *ACS Appl. Mater. Interfaces* **2011**, *3*, 3078−3083.
(29) Piao, Y. Z.; Kim, H. S.; Sung, Y. E.; Hyeon, T. *Chem. Commun.* **2010**, *46*, 118−120.
(30) Kang, E.; Jung, Y. S.; Cavanagh, A. S.; Kim, G. H.; George, S. M.; Dillon, A. C.; Kim, J. K.; Lee, J. *Adv. Funct. Mate.* **2011**, *21*, 2430−2438.
(31) Siriwardene, R. V.; Cook, J. M. *J. Colloid Interface Sci.* **1985**, *108*, 414−422.
(32) Sevilla, M.; Fuertes, A. B. *Carbon* **2006**, *44*, 468−474.
(33) Lee, K. T.; Jung, Y. S.; Oh, S. M. *J. Am. Chem. Soc.* **2003**, *125*, 5652−5653.
(34) Derrien, G.; Hassoun, J.; Panero, S.; Scrosati, B. *Adv. Mater.* **2007**, *19*, 2336−2340.
(35) Zhang, W. M.; Hu, J. S.; Guo, Y. G.; Zheng, S. F.; Zhong, L. S.; Song, W. G.; Wan, L. J. *Adv. Mater.* **2008**, *20*, 1160−1165.
(36) Wu, X. L.; Guo, Y. G.; Wan, L. J.; Hu, C. W. *J. Phys. Chem. C* **2008**, *112*, 16824−16829.
(37) Morimoto, H.; Tobishima, S.; Iizuka, Y. *J. Power Sources* **2005**, *146*, 315−318.
(38) Hang, B. T.; Doi, T.; Okada, S.; Yamaki, J. I. *J. Power Sources* **2007**, *174*, 493−500.
(39) Kostecki, R.; Schnyder, B.; Alliata, D.; Song, X.; Kinoshita, K.; Kotz, R. *Thin Solid Films* **2001**, *396*, 36−43.
(40) Teixidor, G. T.; Zaouk, R. B.; Park, B. Y.; Madou, M. J. *J. Power Sources* **2008**, *183*, 730−740.
(41) Kang, Y. M.; Kim, K. T.; Lee, K. Y.; Lee, S. J.; Jung, J. H.; Lee, J. Y. *J. Electrochem. Soc.* **2003**, *150*, A1538−A1543.
(42) Kang, Y. M.; Kim, K. T.; Kim, J. H.; Kim, H. S.; Lee, P. S.; Lee, J. Y.; Liu, H. K.; Dou, S. X. *J. Power Sources* **2004**, *133*, 252−259.
(43) Kang, Y. M.; Park, M. S.; Song, M. S.; Han, Y. S.; Lee, J. Y. *Mater. Chem. Phys.* **2007**, *105*, 245−249.
(44) Hu, J. Q.; Wen, Z. H.; Wang, Q.; Yao, X.; Zhang, Q.; Zhou, J. H.; Li, J. H. *J. Phys. Chem. B* **2006**, *110*, 24305−24310.
(45) Chen, G.; Wang, Z. Y.; Xia, D. G. *Chem. Mater.* **2008**, *20*, 6951−6956.
(46) Lee, G. H.; Park, J. G.; Sung, Y. M.; Chung, K. Y.; Il Cho, W.; Kim, D. W. *Nanotechnology* **2009**, *20*, 295205.
(47) Kim, J.; Chung, M. K.; Ka, B. H.; Ku, J. H.; Park, S.; Ryu, J.; Oh, S. M. *J. Electrochem. Soc.* **2010**, *157*, A412.
(48) Tarascon, J. M.; Armand, M. *Nature* **2001**, *414*, 359−367.